



This is a repository copy of *Investigation of ignition process from visible to infrared by a high speed colour camera*.

White Rose Research Online URL for this paper:
<http://eprints.whiterose.ac.uk/103880/>

Version: Accepted Version

Article:

Wang, Y., Zheng, L., Woolley, R. et al. (1 more author) (2016) Investigation of ignition process from visible to infrared by a high speed colour camera. *Fuel*, 185. pp. 500-507. ISSN 0016-2361

<https://doi.org/10.1016/j.fuel.2016.08.010>

Article available under the terms of the CC-BY-NC-ND licence
(<https://creativecommons.org/licenses/by-nc-nd/4.0/>)

Reuse

This article is distributed under the terms of the Creative Commons Attribution-NonCommercial-NoDerivs (CC BY-NC-ND) licence. This licence only allows you to download this work and share it with others as long as you credit the authors, but you can't change the article in any way or use it commercially. More information and the full terms of the licence here: <https://creativecommons.org/licenses/>

Takedown

If you consider content in White Rose Research Online to be in breach of UK law, please notify us by emailing eprints@whiterose.ac.uk including the URL of the record and the reason for the withdrawal request.



eprints@whiterose.ac.uk
<https://eprints.whiterose.ac.uk/>

Investigation of Ignition Process from Visible to Infrared by a High Speed Colour Camera

Y. Wang¹, L. Zheng¹, R. Woolley¹, Y. Zhang* (✉)¹

¹ Department of Mechanical Engineering, the University of Sheffield, Sir Frederick Mappin
Building, Mappin Street, Sheffield, S1 3JD, UK

Emails:

ywang30@sheffield.ac.uk

lzheng2@sheffield.ac.uk

rob.woolley@sheffield.ac.uk

yz100@sheffield.ac.uk

Corresponding Author: Yang Zhang, Department of Mechanical Engineering, the University of
Sheffield, Sir Frederick Mappin Building, Mappin Street, Sheffield, S1 3JD, UK

Emails: yz100@sheffield.ac.uk

Phone: +44(0)114 2227880

Fax: +44(0)114 2227890

Abstract

From the image processing of high speed colour images of flame ignition, areas of dominant infrared emission have been noticed, which has stimulated the more in depth investigation in this paper. Two test cases for propane and methane with co-flow air were carried out. By applying selective digital image enhancement technique, the weak chemiluminescence-induced visible flame and infrared signals are simultaneously resolved together with the much stronger visible soot radiation. It is found that the pockets of soot only emitting infrared signal exists in both propane and methane ignition process cases. In the ignition process, the chemiluminescence-induced blue flame is observed first, which is followed by soot only having infrared emission. The visible orange coloured sooty flame only appears afterwards. The soot only emitting infrared is found in between the blue flame and the visible sooty flame. The co-flow air is found to accelerate the ignition process and it also brings forward soot formation. The investigation demonstrates that a proper image enhancement technique is essential in the further understanding of combustion process taking place when using a high speed camera.

Keywords: Image enhancement; Infrared emission; Ignition process; Flame colour; Soot radiation

1. Introduction

The ignition of burner flames has been shown to be sensitive to ignition system [1], fuel flow rate and ignition location [2-4]. A good understanding of this process can be achieved through simultaneous multispectral time dependent visualisation of both the ignition physics and subsequent combustion. As a result, sophisticated experiments remain essential to enhance our understanding. Laser imaging is often used to study the flame development during the ignition process. For example, particle image velocimetry (PIV) and planar laser-induced fluorescence (PLIF) techniques can simultaneously provide fluid velocity field conditions, radical (CH, OH, NO, etc.) distributions, flame structure and stability [5-7]. Ahmed and Mastorakos [2] applied OH-PLIF to study ignition and followed the edge flame propagation in turbulent non-premixed methane flames. They reported that the flame kernel growth rate increased with higher spark energy, thinner electrode diameter and wider gap. However, these techniques remain expensive to implement and the optical access required may result in a significant redesign of the combustion chamber.

Typical hydrocarbon flame consists of the broad band orange coloured soot particle radiation and spectral band emission of excited species in the ultra violet (UV), visible and infrared spectrums [8]. In the visible spectrum excited molecular radicals CH* (430 nm) and C₂* (Swan system, dominant emissive band head at 473.71 nm and 516.52 nm) produce 'blue' light [9], the intensity of which has been demonstrated to vary with fuel composition, flow rate, and heat release rate [10-12]. The ratio of CH*/C₂* can be used to determine the local equivalence ratio [13]. Orange coloured flames are produced by grey-body radiation of incandescent soot. Soot formation occurs via precursor species which mainly consist of polycyclic aromatic hydrocarbons (PAH) [14]. Subsequently, small particles are formed through chemical coagulation. As the soot particles travel through an oxidizing region, soot formation ceases. Within the UV, the hydroxyl radical, OH* has the strongest band with the primary head at 309 nm [8]. Emission in the infrared spectrum has two primary components various emission bands and continuum radiation. The strongest band is around 4.4 μ m due to CO₂, and there is another

strong band at $2.8\mu\text{m}$ as a result of emission from both CO_2 and H_2O [9]. The continuum radiation from heated soot particles in the flame has a peak emission in the mid infrared region of the spectrum [15].

The flame ignition process studies are generally relied on high speed cameras. Research indicated soot emission tends to obscure the CH^* and C_2^* signals at high shutter speeds [16, 17]. Directed high speed imaging from the Rolls-Royce gas-turbine combustor seems to indicate that the flame is discontinuous during the ignition process [18]. However, through selective image enhancement technique Huang and Zhang reveal that there exists very weak visible blue coloured flame in the seemingly flameless image sequence. In our recent tests it is found that pockets of flame that only emits in the infrared spectrum can be detected by some high speed cameras besides the visible flame emission, which has not been reported before. Although Kapaku et al. [19] visualised soot and carbon dioxide radiation intensity of an ethylene diffusion flame using a high-speed mid-infrared camera with two band-pass filters, only infrared emissions were recorded instead of both the visible and infrared. Huang and Zhang [20] imaged a methane flame under various stable burning conditions with an Olympus E-100RS digital camera. In the investigation of the infrared emission, an infrared filter was applied. They found that the infrared emission distribution detected by the camera did not overlap with the visible flame colour in the hue space. Hue is referred to the colour appearance which is related to the spectrum [21]. However, the objective of the study focused on the stable flame and the infrared emission was not resolved simultaneously with the visible flame.

In a recent investigation of ignition, it was noted that infrared emission was detected despite the fact that a high speed colour digital cameras usually have an infrared cut-off filter. With the aid of selective digital image enhancement techniques [20], the visible CH^* and C_2^* and the infrared emission were segmented, enhanced and visualised. Therefore a single digital high speed colour camera combined with selective digital image enhancement can be used to investigate the flame ignition process in both the visible to the infrared spectrum. In this work, the temporal ignition development of flames above

fuel jets was captured and the evolving light emission from the flame was analysed.

2. Experimental procedure

2.1 Experimental setup

The ignition process was captured by a high speed camera (Photron FASTCAM SA4) with a full frame resolution of 1024 by 1024 pixels. A sigma 24-70 mm lens is applied to the camera. The aperture is set as f/2.8 in all the cases. The ignition was initiated with a Kawasaki ignition-coil (TEC-KP02), with approximately an output voltage of 30 kV. The spark was created between a pair of steel electrodes separated by a 9 mm gap. A schematic of the experimental setup is shown in Fig. 1.

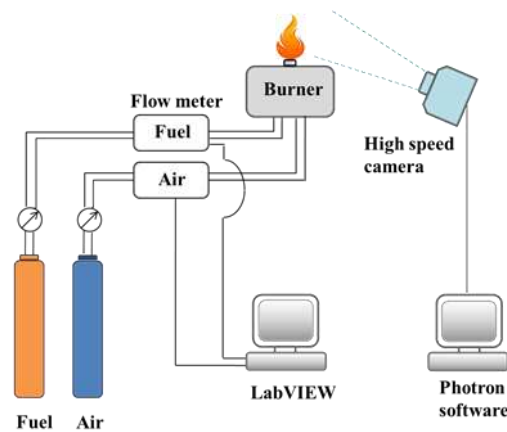


Fig. 1. The schematic experimental setup.

Two test cases were investigated. In Test Case 1, a free propane non-premixed flame jet was established. The gas flow rate was regulated by a mass flow controller. The fuel was injected through a nozzle of 9.6 mm diameter. The fuel jet flow rate was 5 l/min, which corresponds to fuel jet velocity of 1.15 m/s and Reynolds number (Re) of 2451. The spark electrodes were located 90 mm above the fuel nozzle. In Test Case 2, non-premixed methane flames with co-flow air were investigated. The fuel was injected through a central nozzle of 18.28 mm diameter. Co-flow air surrounded the fuel in a coaxial condition. A fine meshed honeycomb was placed inside the nozzle to straighten the air. The detailed structure of the burner can be found in [22]. The co-flow air nozzle diameter was 37.8 mm.

The fuel flow rate was 0.182 l/min which corresponding to a fuel Reynolds number of 55.4. Three co-flow air flow rates 0 l/min, 14 l/min ($Re=479$) and 75 l/min ($Re=2565$) were used. The electrodes were fixed at a distance of 14 mm above the nozzle.

2.2 Colour identification from visible to infrared spectrum

Although filters are installed to block infrared emission, the high speed camera (Photron SA4) is still sensitive in the near infrared (NIR) region. To verify that the camera is able to capture the infrared emission from the flame, a Pentax stereo adaptor [23] (Fig. 2), is applied to the front of the lens, which generates two parallel images with slight displacement.



Fig. 2. A Pentax stereo adaptor.

Different filters can be applied to the left and right views. The left view without any filter directly captured the flame images. A wideband filter (385 - 725nm wavelength, transmittance $> 96\%$) is applied to the right view which allows the visible light to pass through only. An example of flame synchronous images pair and their corresponding colour distribution histograms in hue space are shown in Fig. 3 (a) and (b) respectively. The x-axes of the histograms indicate the hue domain. The y-axes are the ratio of intensity which corresponds to a specific hue range over total pixel intensity of the image. The pixel intensity represents the brightness of the pixel. The intensity threshold of pixel intensity is 0 to 2^{16} in all the captured images presented in this paper. It is found that the flame image without the filter has an additional region which surrounds the orange sooty flame, and its colour distribution locates from H2 to H18. The image with visible wideband filter dominates the hue domain

from H2 to H13. It has been tested that the Photron SA4 camera can not detect the ultra-violet signals with the applied camera settings. Therefore the colour distribution from H14 to H18 has to be infrared signals from the flame. It should be noted that the presented flame images are post-processed through a selective enhancement technique which is introduced in Section 2.3. The original images are analysed to plot histograms.

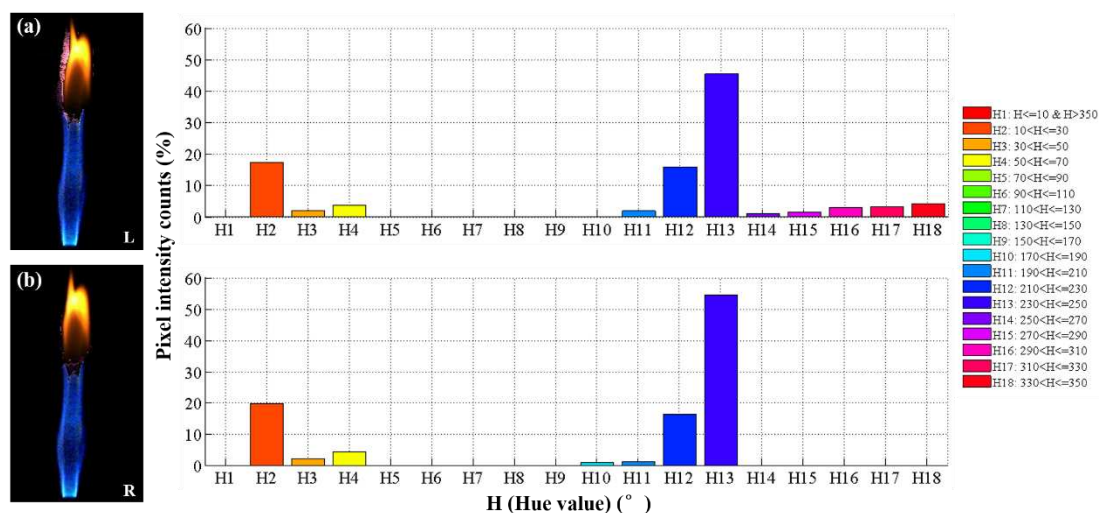


Fig. 3. The synchronous images of propane partially premixed flame (a) without a filter and (b) with a visible wideband filter (385nm - 725nm wavelength) and their corresponding colour distribution histograms in hue space. The number of pixels of the flame images is 18795 and 17126 respectively.

Shown in Fig. 3 (a), the infrared emission band occurs behind the CH* and C2* emission region but slightly ahead of the soot emission. It is thought that the emission from the H14 to H18 bands is associated with the soot formation process. Additional experiments have been conducted on lean premixed propane/ air and methane/ air flames. The captured images and corresponding colour distribution histograms in hue space are shown in Fig. 4 (a) and (b). It is found that the pixel intensity counts concentrate in chemiluminescence-induced blue flame region. The emission from H14 to H18 (< 0.5%) is negligible, which means this is unlikely to be emission from the infrared bands from either CO₂ or H₂O. Another experiment of a propane diffusion flame is developed as shown in Fig. 4 (c). The flame infrared emission is found at the outer layer which surrounds the orange sooty flame. Dark smoke can be seen surround the flame and then gradually rises during the experiment, which further

demonstrates that the region of infrared emission only are low-temperature soot and dominates the hue domain from H14 to H18.

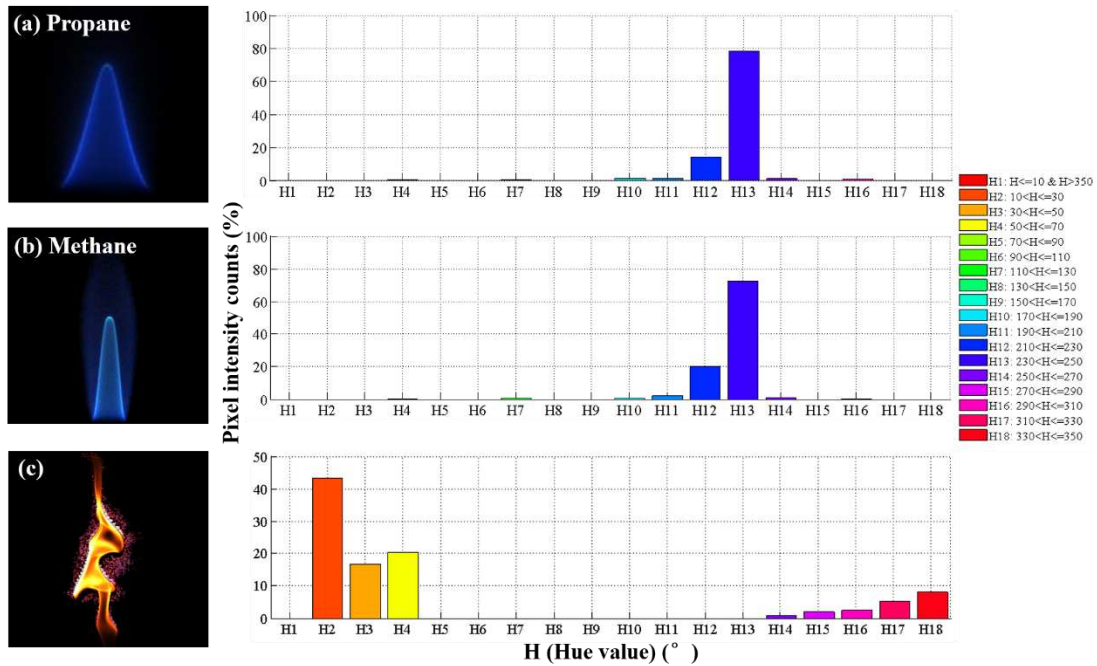


Fig. 4. The captured images of lean premixed (a) propane/ air flame; (b) methane/ air flame at equivalence ratio $\Phi=0.98$ and the corresponding colour distribution histograms in hue space. The number of pixels of the flame images is 2011 and 3711 respectively. (c) The captured image of propane diffusion flame and the corresponding colour distribution histogram in hue space. The number of pixels of the flame image is 71794.

2.3 Selective digital image enhancement method

Fig. 5. (a) is the original image at a shutter speed of 1/2000 s of propane non-premixed flame at 0.102s after ignition. Both blue flame region (CH^* and $C2^*$) and infrared emission signals are weak in comparison with the orange-coloured soot emission. As a result, selective digital image enhancement [18, 20] is essential. After image post-processing, the blue flame colorations of the captured images are filtered within the hue value band from 180° to 252° in the Hue Saturation Value (HSV) colour model space and then enhanced 20 times; the region of infrared emission only is filtered from 252° to 330° and then enhanced 15 times. The noise from the camera and background is removed. Figs. 5 (a)

and (e) compare the original and the combination of selective enhanced flame images demonstrating the usefulness of selective image enhancement in revealing the real physical process. Here the arbitrary values of 15 and 20 are only chosen for enhanced visualisation. The original values are chosen for quantitative analysis.

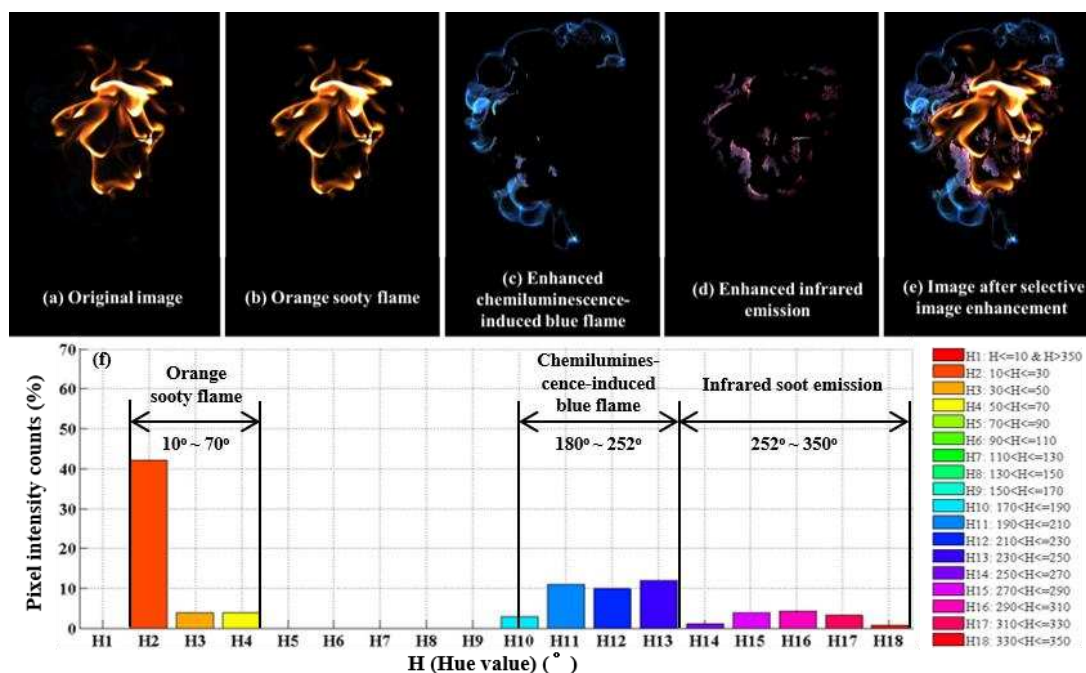


Fig. 5. (a) The original image at a shutter speed of 1/2000 s; (b) the orange sooty flame region; (c) the chemiluminescence-induced blue flame which is enhanced 20 times; (d) the infrared soot emission which is enhanced 15 times; (e) the entire image after selective image enhancement; (f) the colour distribution histogram in hue space of propane non-premixed flame at 0.102s after ignition. The number of pixels of the flame images from (a) to (e) is 162012, 83022, 57752, 21238 and 162012 respectively.

3. Results and discussion

In order to investigate the ignition process of different fuels, two test cases for propane and methane are conducted. In Test Case 2, co-flow air is introduced to study its effects, such as timespan of ignition process, variation of chemiluminescence-induced blue flame and sooty flames and fuel-air mixture condition.

3.1 Ignition process of free jet propane non-premixed flame

In Test Case 1, the high speed digital camera captured the flame at 1000 frames per second with 1/2000 s shutter speed. Figs. 6 (a) and (b) show the original and selective enhanced image sequences. Fig. 7 gives the time-dependent number of pixels of the soot-induced orange flame, infrared emission and the chemiluminescence-induced blue flame in the given hue band. The number of pixels is used to define the area of the different flame colour region. A small spherical blue flame is observed to form at approximately 0.005s. As the flame grows, the infrared emission of soot can be observed after the formation of the CH* and C2* at the flame front. The outer layer fuel is ignited at well-mixed fuel-air mixture condition, and provides a high temperature blue flame front surrounding partially oxidised fuel. The hot gas of the combustion products blocks/slows the air mixing path to the encircled fuel pocket. In the preheating zone, the fuel is heated by heat conduction and heat diffusion of the high temperature combustion product, which results in the pyrolysis of the propane and forms the carbon soot at the centre [24]. The grey body radiation in the infrared spectrum of the soot contributes to the flames pinkish appearance in the captured images. It should also be stressed that the pink region is only emitting infrared. The orange-coloured soot region should also have infrared component but it is shadowed by the visible light signals. At 0.012s, a typical orange diffusion flame appears in the centre of the flame ball due to incandescent soot rising to a higher temperature. The orange flame and infrared emission increase rapidly from 0.117s as shown in Fig. 7, the result of the bottom of the flame attaching to the fuel nozzle exit. The fuel then jets through the flame inner zone and more soot accumulates at the centre of the flame and enlarges the soot-induced orange flame and infrared emission regions. Subsequently, the sooty flame expands and encompasses the outer premixed flame. At 0.152s after ignition, the blue flame region completely vanishes in the upper part of the flame and is concentrated close to the nozzle. At 0.196s, the number of blue coloured flame pixels becomes zero, while the number of infrared sooty flame pixels keeps increasing. Therefore the infrared sooty flame is unlikely to be a combination of blue coloured flame and orange sooty flame.

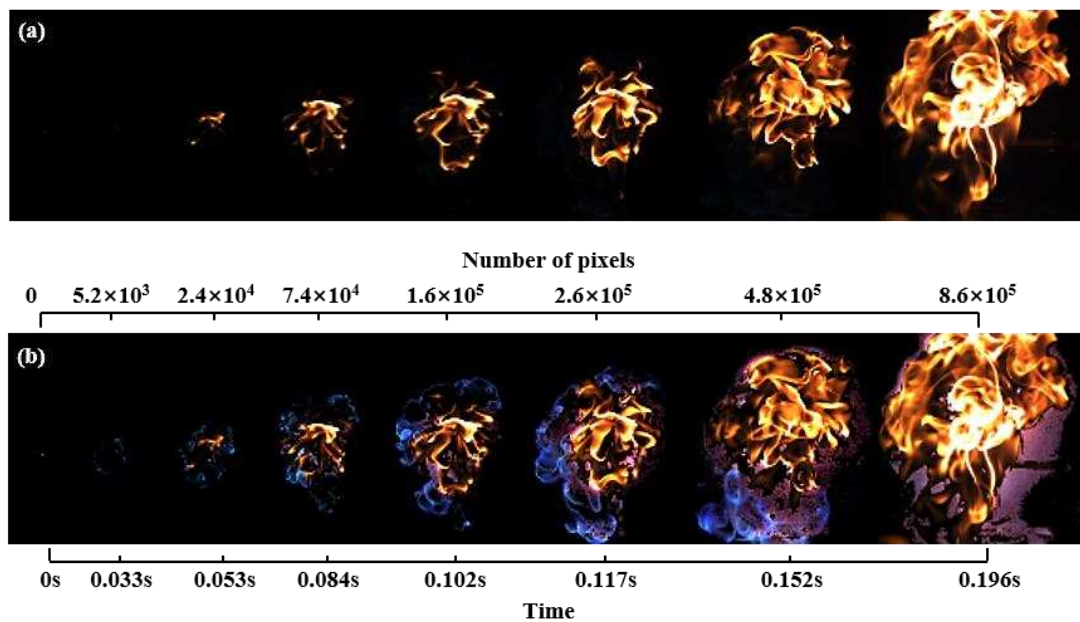


Fig. 6. (a) The original and (b) selective enhanced image sequences of ignition process of propane non-premixed flame with corresponding number of pixels.

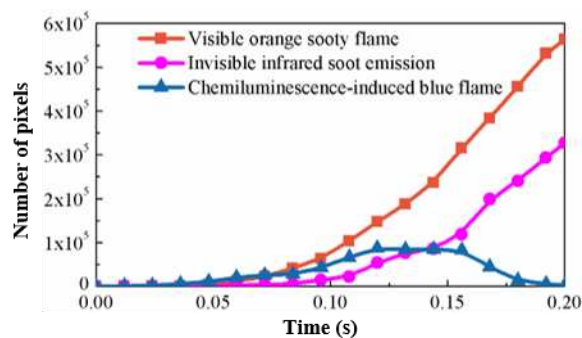


Fig. 7. The time-dependent number of pixels of the soot-induced orange flame, infrared emission only soot pockets and the chemiluminescence-induced blue flame.

3.2 Ignition process of methane non-premixed jet flame with different co-flow air flow rates

Here, the ignition processes of methane non-premixed jet flame at 0 l/min, 14 l/min and 75 l/min co-flow air were investigated (referred to as 'Pure methane', 'Air 14' and 'Air 75' respectively). The high speed camera was set at 500 frames per second with a 1/500 s exposure time. The intensity of the weak blue flame is enhanced 25 times, and the infrared emission is enhanced 30 times in Fig. 8 where enhanced flames are shown for all three conditions.

Shown in Fig. 8 (a), a blue flame with a bright tip stretches and propagates in the jet axial direction at the early stage of ignition. At 0.032s, infrared emission can be observed inside the blue flame primarily located around the electrodes and near the tip of the flame. At 0.050s after ignition, a soot-radiation-induced orange flame forms inside the infrared sooty flame pocket. The orange flame region rapidly grows and dominates most of the area inside the blue premixed flame. It changes colour from weak orange to bright yellow indicating that the temperature is increasing. In the meantime, the soot only having infrared emission region becomes a thin layer between the blue and orange emission regions. The bright blue flame tip then gradually separates from the main structure of the flame. At 0.078s, a sooty orange flame with outer layer infrared emission emerges from the broken blue flame pocket. Subsequently, the flame necking occurs due to the buoyancy [25]. The soot which is concentrated in the upper section of the flame emerges from the main structure and propagates upwards, then gradually burns out. Finally, a cone-shaped flame stabilised on the nozzle exit can be observed at 0.114s after ignition. This short stable flame is formed with blue bottom, yellow top and soot only having infrared emission in between.

When 14 l/min co-flow air is introduced, a tulip flame is formed at the beginning of ignition process as shown in Fig. 8 (b). The phenomenon is similar to 'Pure methane'. However, the initial blue flame region is narrower and the infrared emission only forms near the tips of the electrodes. For co-flow air of 75 l/min, the orange sooty flame region is not observable, see Fig 8 (c). Only the blue flame with a little infrared emission is observed. A blue flame forms first, and then the infrared emission occurs at 0.006s after ignition. At 0.018s, the infrared emission disappears and then reappears at 0.048s when the flame necking occurs. At 0.084s, the flame becomes stable with a blue appearance and a little infrared emission inside. It is found that with the increase of the co-flow rate, the tip of the final stable flame becomes sharper.

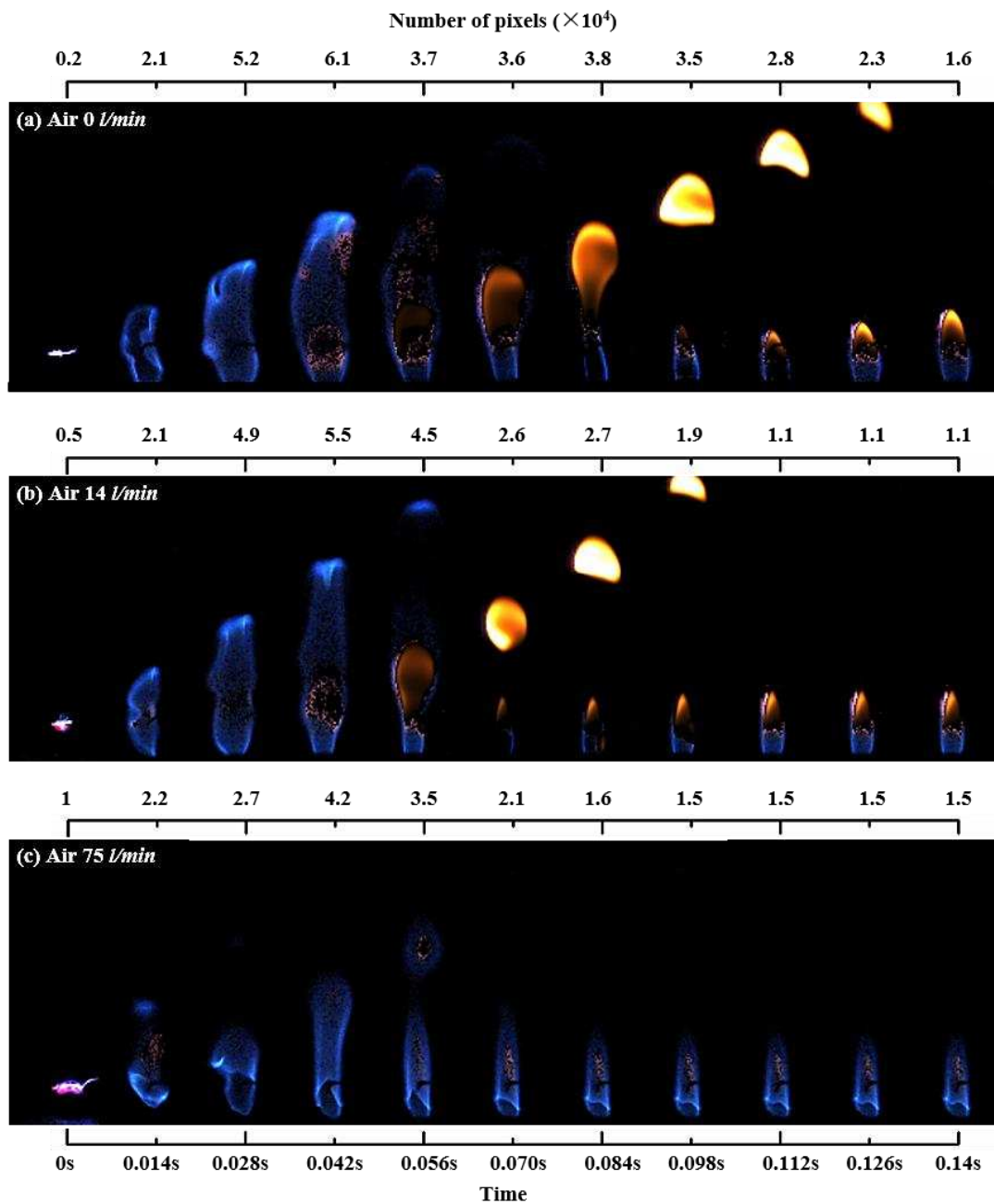


Fig. 8. (a)-(c) The enhanced image sequences of ignition processes with corresponding number of pixels of 'Pure methane', 'Air 14' and 'Air 75' respectively.

Shown in Figs. 9 (a)-(c) are the time-dependent number of pixels of the soot-induced orange flame, infrared emission and the chemiluminescence-induced blue flame for the pure methane and co-flow flames. The trends for 'Pure methane' and 'Air 14' are similar. Infrared emission occurs prior to the generation of soot induced orange emission. At the early stage, as co-flow is introduced the number of chemiluminescent pixels decreases as the flame length decreases and soot formation occurs sooner.

The flame also takes less time to reach a steady state when increasing the co-flow air velocity. Moreover, the peak values of accumulative of orange flame and infrared emission become smaller as the co-flow air increases which indicates that the co-flow air enhances the air/fuel mixing and reduces the quantity of soot formation.

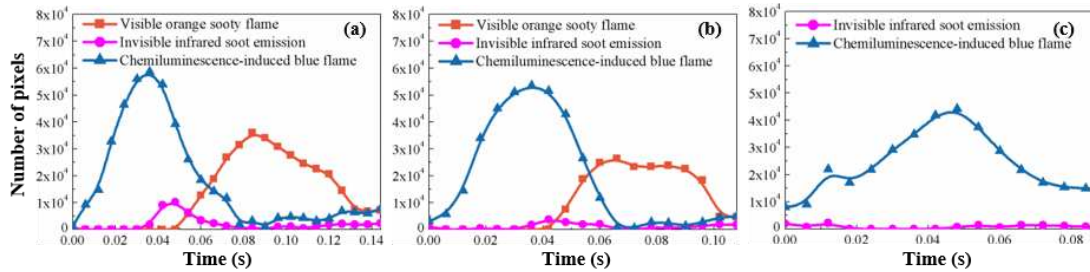


Fig. 9. (a)-(c) The time-dependent number of pixels of the soot-induced orange flame, infrared emission only soot pockets and the chemiluminescence-induced blue flame of ‘Pure methane’, ‘Air 14’ and ‘Air 75’ respectively.

Shown in Figs. 10 (a) and (b) are the time-dependent mean intensities of the soot-induced orange flame and the infrared emission regions. The mean intensity is the ratio of total pixel intensities over the total number of pixels. For a single image, even some pixels with the same hue value, their intensities may be different. Combined with the flame colour division in hue domain, the mean intensity is used to describe an average pixel brightness of specified flame region (e.g. soot-induced orange flame region). The intensity of soot-radiation reflects the flame temperature [26]. In Fig. 10 (a) the intensity for the ‘Pure methane’ can be seen to increase soonest which indicates a significant rise in the temperature. After that, the intensity drops when the high temperature soot which is concentrated in the upper section of the flame emerges from the base of the flame and then burns out. The curve of ‘Air 14’ shows a similar trend but the intensity is weaker. The mean intensities of infrared soot emission reduce with the increase of the air flow rate when the flame reaches a steady state.

Fig. 10 (c) shows the time-dependent blue/green intensity ratio of the blue flame region. Huang and Zhang [27, 28] introduced a Digital Flame Colour Discrimination (DFCD) combustion quantification

scheme, which established a relation between the different flame radiation components and its colour signal presence. The intensity ratio of the B/G (in the RGB colour space) was shown to indicate the global air/fuel mixture condition [17] and equivalence ratio [29] of the blue flame region. In Fig. 10 (c), the curves of ‘Pure methane’ and ‘Air 14’ initially decrease, which indicates the ignition condition moves towards fuel rich condition. The curves then increase due to further mixing with the air. The curve of ‘Air 75’ is nearly flat that means the fuel and air mixing state is constant. In the beginning, the curve of ‘Air 75’ is higher than the others which indicating a leaner local burn. The initial lower infrared soot and no orange coloured sooty flame for ‘Air 75’ in Figs. 10 (b) and (a) also support this.

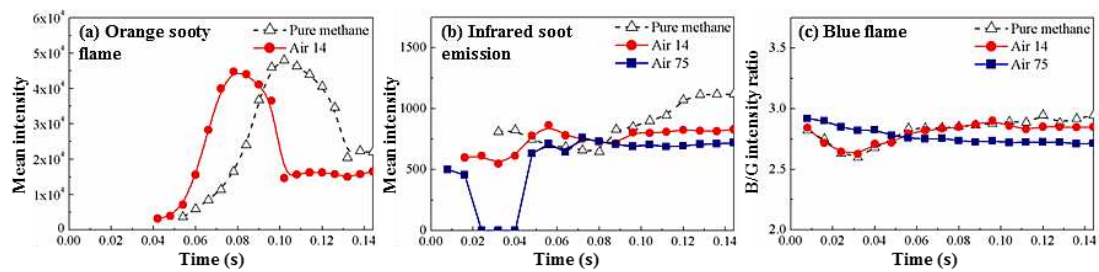


Fig. 10. The time-dependent mean intensities of the (a) soot-induced orange flame and the (b) infrared emission only regions. (c) Blue/green intensity ratios of the chemiluminescence-induced blue flame.

Fig. 11 shows the comparisons of ‘Air 14’ repeat test results, which demonstrate a reasonable repeatability of the tests, and similar reproducibility was observed for other attempts.

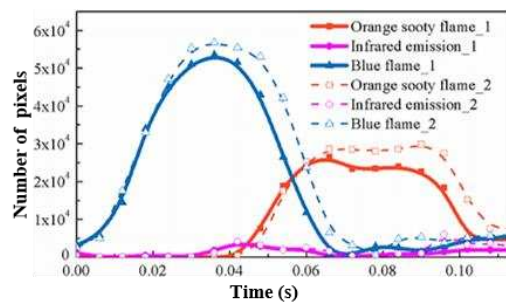


Fig. 11. Comparisons of ‘Air 14’ repeated test results: The time-dependent number of pixels of the soot-induced orange flame, infrared emission only soot pockets and the chemiluminescence-induced blue flame.

4. Conclusions

The ignition processes of a) a propane non-premixed free jet flame, and b) non-premixed methane jet with different flow rates of co-flow air have been investigated via a single high speed digital colour camera. Without enhancement, the images are dominated by ‘orange-coloured’ soot emission. The weaker chemiluminescence-induced blue flame and infrared signals have to be resolved through selective digital image enhancement techniques. As a result, the simultaneous visualisations and investigation of flame emission from the visible to a limited infrared spectrum in a single image have been achieved. The results demonstrate that there exists a region of infrared emission only between the chemiluminescence and ‘orange’ pockets. This has been demonstrated both spatially and temporally in propane non-premixed free jet flame and in the co-flow methane flame. The infrared emission is thought to be associated with the pyrolysis of the fuel rich mixture when it is surrounded by hot flame or combustion products. In the case of non-premixed methane jet, the co-flow air is found to accelerate the ignition process and shorten the ignition time. When the flow rate of the co-flow air was increased, the formation of infrared and orange sooty flame occurred earlier in the ignition process. Furthermore, the increase of the flow rate of the co-flow air affects the variation of the fuel and air mixture state in the ignition process. The research has demonstrated that direct high speed imaging and visualisation can be misleading due to the large disparity in signal strength of the various flame light emission. Much more physical insights can be gained into the combustion process if a modern high speed colour camera is combined with innovative image processing technique.

Acknowledgments

The research is partly benefited from the EPSRC projects: [EP/K036750/1](#) and [EP/G063044/1](#).

References

- [1] E. Mastorakos, *Progress in Energy and Combustion Science* 35 (1) (2009) 57-97.
- [2] S. F. Ahmed, E. Mastorakos, *Combustion and Flame* 146 (1-2) (2006) 215-231.
- [3] Y. Zhang, K.N.C. Bray, *Combustion and Flame* 116 (4) (1999) 671-674.
- [4] C. McDaid, J. Zhou, Y. Zhang, *Fuel* 103 (2013) 783-791.
- [5] J. Hult, U. Meire, W. Meier, A. Harvey, C.F. Kaminski, *Proceedings of the Combustion Institute* 30 (2005) 701-709.
- [6] I. Boxx, C. Heeger, R. Gordon, B. Böhm, M. Aigner, A. Dreizler, W. Meier, *Proceedings of the Combustion Institute* 32 (1) (2009) 905-912.
- [7] C. Heeger, B. Böhm, S.F. Ahmed, R. Gordon, I. Boxx, W. Meier, A. Dreizler, E. Mastorakos, *Proceedings of the Combustion Institute* 30 (2005) 701-709.
- [8] A. G. Gaydon, *The Spectroscopy of Flames*, Chapman and Hall, London, 1974, p. 10, 144.
- [9] A. G. Gaydon, *The Spectroscopy of Flames*, Chapman and Hall, London, 1974, p. 221.
- [10] T. García-Armingol, J. Ballester, *International Journal of Hydrogen Energy* 39 (21) (2014) 11299-11307.
- [11] J. Kojima, Y. Ikeda, T. Nakajima, *Proceedings of the Combustion Institute* 28 (2) (2000) 1757-1764.
- [12] C.S. Panoutsos, Y. Hardalupas, A.M.K.P. Taylor, *Combustion and Flame* 156 (2) (2009) 273-291.
- [13] B.N. Raghunandan, C. Oommen, R.K. Sullerey. *Air breathing Engines and Aerospace Propulsion Proceedings of NCABE*, Indian Institute of Technology Kanpur, Pvt. Ltd, India, 2004, p. 32.
- [14] S. Turns, *An Introduction to Combustion: Concepts and Applications*, McGraw-Hill Higher Education, New York, 2011, p. 343-344.
- [15] W.C. Kim, Y.R. Sivathanu, J.P. Gore, *Conference on Automatic Fire Detection*, National Institute of Standards and Technology, U.S.A., 2001.
- [16] Q. Wang, H.W. Huang, Y. Zhang, C.Y. Zhao, *Fuel*, 108 (2013) 177-183.
- [17] Q. Wang, C.Y. Zhao, Y. Zhang, *Experimental Thermal and Fluid Science*, 62 (2015) 78-84.

- [18] H.W. Huang, Y. Zhang, *Measurement Science and Technology*, 22 (7) (2011).
- [19] R.K. Kapaku, B.A. Rankin, J.P. Gore, *Combustion and Flame* 162 (10) (2015) 3704-3710.
- [20] H.W. Huang, Y. Zhang, *Measurement Science and Technology*, 19 (8) (2008).
- [21] A. Choudhury, *Principles of Colour Appearance and Measurement*, Woodhead Publishing Limited in association with The Textile Institute, Cambridge, U.K., 2014, p. 124.
- [22] Q. Wang, H. Gohari Darabkhani, L. Chen, Y. Zhang, *Experimental Thermal and Fluid Science*, 37 (2012) 84-90.
- [23] W.B. Ng, Y. Zhang, *Experiments in Fluids*, 34 (2003) 484-493.
- [24] A.W. Castleman, J.P. Toennies, K. Yamanouchi, W. Zinth, in: H. Bockhorn (Ed), *Soot Formation in Combustion: Mechanisms and Models*, Springer Series in Chemical Physics, 1994, p. 5-7.
- [25] J.S. Turner, *Buoyancy Effects in Fluids*, Cambridge University Press, U.K., 1973, p. 94.
- [26] M.K. Chernovsky, A. Atrey, K.R. Sacksteder, 44th AIAA Aerospace Sciences Meeting and Exhibit, American Institute of Aeronautics and Astronautics, Nevada, U.S.A., 2006.
- [27] H.W. Huang, Y. Zhang, *Fuel*, 90 (1) (2011) 48-53.
- [28] H.W. Huang, Y. Zhang, *International Journal of Hydrogen Energy*, 38 (1) (2013) 4839-4847.
- [29] J.S. Yang, F.M.S. Moss, H.W. Huang, Q. Wang, R. Woolley, Y. Zhang, *Proceedings of the Combustion Institute*, 35 (2) (2015) 2075-2082.